Photonic Which-Path Entangler Based on Longitudinal Cavity-Qubit Coupling

Z. M. McIntyre* and W. A. Coish†
Department of Physics, McGill University, 3600 rue University, Montreal, Québec H3A 2T8, Canada

(Received 22 June 2023; revised 6 December 2023; accepted 29 January 2024; published 28 February 2024)

We show that a modulated longitudinal cavity-qubit coupling can be used to control the path taken by a multiphoton coherent-state wave packet conditioned on the state of a qubit, resulting in a qubit–which-path (QWP) entangled state. QWP states can generate long-range multipartite entanglement using strategies for interfacing discrete- and continuous-variable degrees of freedom. Using the approach presented here, entanglement can be distributed in a quantum network without the need for single-photon sources or detectors.

DOI: 10.1103/PhysRevLett.132.093603

Fault-tolerant quantum computing will require redundancy to identify and correct errors during a computation. In most architectures, the physical qubits will therefore vastly outnumber the logical qubits. The need to scale up existing architectures has motivated a network approach where remote qubits, grouped into nodes, are connected by quantum-photonic interconnects [1–5]. These quantum networks naturally require entanglement distribution across nodes. Consequently, significant effort has gone towards generating both heralded [6–12] and deterministic [13–20] qubit-photon entanglement.

In this Letter, we present a photonic which-path entangler that correlates the path of an incoming multiphoton coherent-state wave packet with the state of a cavity-coupled control qubit (Fig. 1). The resulting which-path degree of freedom, consisting of a coherent-state wave packet traveling in one of two transmission lines, can be reencoded in the photon-number parity of a continuous-variable degree of freedom, then used to generate entanglement with one or more distant qubits. The entangler presented here therefore provides a natural interface between discrete- and continuous-variable approaches to hybrid quantum computation [21–26]. The qubit–which-path (QWP) state generated by the entangler also has greater potential sensitivity for phase measurements than either the comparable entangled coherent state (ECS) [27,28] (consisting of a superposition of coherent states, one in each interferometer arm) or NOON state [29–31] (an analogous superposition of N-photon Fock states). Quantum-enhanced interferometry has applications in, e.g., biological imaging [32–34] and gravitational wave detection [35–38].

A key requirement for the entangler is a modulated longitudinal (qubit-eigenstate preserving) cavity-qubit coupling. Longitudinal coupling has attracted significant theoretical and experimental attention in recent years, as it is currently being realized and leveraged in a number of promising quantum-computing architectures [39–49]. Though many current implementations of, e.g., cavity-coupled spin, charge, and superconducting qubits make use of the (transverse) Rabi coupling, longitudinal cavity-qubit couplings are no less fundamental. They can be engineered for single-electron-spin qubits in double quantum dots (DQDs), which can be coupled to cavity electric fields via magnetic-field gradients [42], as well as for hole-spin qubits in semiconductors [47,49,50], which interact with electric fields via their large intrinsic spin-orbit coupling. Two-electron-spin singlet-triplet qubits in DQDs can be longitudinally coupled to electric fields by modulating a gate voltage controlling the strength of the exchange interaction [45,48]. Longitudinal coupling can also be engineered in various superconducting-qubit architectures [39–41,43,44]. Moreover, even in systems where the dominant source of cavity-qubit coupling is intrinsically transverse, an effectively longitudinal interaction can be engineered (in some rotating frame) by modulating the coupling strength at both the cavity and qubit frequencies [46], making the theory presented here widely applicable.

Model.—A longitudinal cavity-qubit interaction arises, e.g., from the dc Stark shift due to electric dipole coupling ($\propto Ey$ for a cavity electric field E polarized along $\hat{y}$).

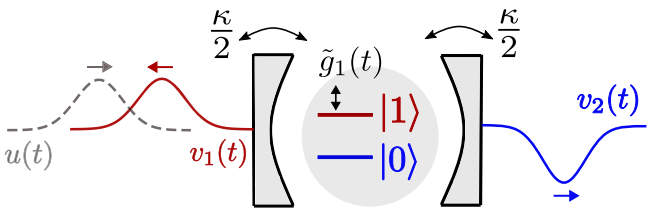

FIG. 1. In the presence of a longitudinal cavity-qubit coupling modulated at the cavity frequency with envelope $\tilde{g}_1(t)$, an incoming coherent state with waveform $u(t)$ is reflected (transmitted) into a coherent state with waveform $v_1(t)$ [$v_2(t)$] for control-qubit state $|1\rangle$ ($|0\rangle$). This effect requires symmetric decay rates $\kappa_1 = \kappa_2 = \kappa/2$ for cavity ports $i = 1, 2$.

 © 2024 American Physical Society

Quantizing the cavity field (focusing on a single cavity mode of frequency ω_c and annihilation operator a), and in adiabatic perturbation theory, we find an interaction proportional to the product of $E \propto i(a^\dagger - a)$ and the dipole matrix element $\langle s(t)|y|s(t)\rangle$ taken with respect to the instantaneous qubit energy eigenstate $|s(t)\rangle$ ($s = 0, 1$) [51]. This gives an effective Hamiltonian $H_{\rm eff}(t) = \sum_s i g_s(t) (a^\dagger - a)|s\rangle\langle s|$, where $|s\rangle$ is a time-independent state in the adiabatic frame, and where $g_s(t) = g_s[\{x_j(t)\}] \propto \langle s(t)|y|s(t)\rangle$ inherits time dependence from a collection of control parameters $\{x_j\}$ that determine $|s(t)\rangle$. For spin qubits, the spin-dependent electric dipole matrix elements [and consequently $g_s(t)$] can be modulated through external electric fields or gate voltages [42,47,49]. An analogous mechanism exists for flux-tunable superconducting transmon qubits, in which the couplings $g_s(t)$ can instead be tuned by modulating a flux [41]. In what follows, we assume a time-independent value $g_0(t) = \bar{g}_0$ and a sinusoidal modulation of $g_1(t)$ at the cavity frequency, $g_1(t) = \bar{g}_1 + 2|\tilde{g}_1(t)| \cos[\omega_c t - \vartheta(t)]$, where $\tilde{g}_1(t) = e^{i\vartheta(t)}|\tilde{g}_1(t)|$ is a slowly varying envelope with $\tilde{g}_1(0) \simeq 0$ and duration τ. (See the Supplemental Material, Ref. [51], for a sufficient condition on the parameters $\{x_j\}$ in general, as well as specific conditions to achieve this coupling modulation for double-quantum-dot charge and spin qubits.) A polaron transformation can then be used to eliminate the term $\propto \bar{g}_0$ by incorporating a small shift $\sim \bar{g}_0^2/\omega_c$ in the qubit frequency ω_q. Going to an interaction picture with respect to the decoupled Hamiltonian $\omega_c a^\dagger a + \omega_q \sigma_z/2$ ($\sigma_z = |0\rangle\langle 0| - |1\rangle\langle 1|$), and within a rotating-wave approximation requiring that $|\bar{g}_1|, |\tilde{g}_1(t)| \ll \omega_c$, the cavity-qubit Hamiltonian is then given by [51]

$$H_0(t) = \frac{\xi(t)}{2}\sigma_z + i|1\rangle\langle 1|[\tilde{g}_1(t)a^\dagger - \text{H.c.}], \tag{1}$$

where we have introduced a stochastic noise parameter $\xi(t)$ leading to qubit dephasing. In general, the dipole approximation also produces a transverse Rabi term $[ig_\perp \sigma_x(a^\dagger - a)]$, which, in the regime $|g_\perp| < |\delta|$ ($\delta = \omega_q - \omega_c$), leads to a dispersive coupling $\chi \sigma_z a^\dagger a$, where $\chi = g_\perp^2/\delta$. Any effects due to transverse coupling can be suppressed by operating in the regime $|g_\perp| \ll |\delta|$.

The longitudinal interaction $\propto \tilde{g}_1(t)$ displaces the cavity vacuum into a finite-amplitude coherent state for $s = 1$. A similar effect is studied in Ref. [41] to design a fast quantum nondemolition (QND) qubit readout. Relative to Ref. [41], we additionally consider driving of the cavity by an input field. In particular, we assume that the cavity is coupled to external transmission lines at input ($i = 1$) and output ($i = 2$) ports (Fig. 1). An input spatiotemporal mode (wave packet) with normalized waveform $u(t)$ [$\int dt|u(t)|^2 = 1$] can be represented by the mode operator $b_u = \int dt\, u^*(t) r_{\text{in},1}(t)$ [63,64], where $r_{\text{in},i}(t)$ satisfies the input-output relation $r_{\text{out},i}(t) = r_{\text{in},i}(t) + \sqrt{\kappa_i} a(t)$ [65]. Here, $r_{\text{out},i}(t)$ is the output field, and κ_i is the rate of decay from cavity port i. We assume that the quantum state of the incoming wave packet is a coherent state with initial amplitude $\langle b_u\rangle = \alpha_0$, giving $\langle r_{\text{in},1}\rangle_t = u(t)\alpha_0$. Where it appears, the notation $\langle \mathcal{O}\rangle_t$ indicates an average with respect to the initial state $\rho(0)$: $\langle \mathcal{O}\rangle_t = \text{Tr}\{\mathcal{O}(t)\rho(0)\}$ for operator $\mathcal{O}$. The reflected and transmitted waveforms are given in the frequency domain by $v_1(\omega) = R(\omega)u(\omega)$ and $v_2(\omega) = T(\omega)u(\omega)$, respectively, where $R(\omega) = \langle r_{\text{out},1}\rangle_\omega / \langle r_{\text{in},1}\rangle_\omega$ and $T(\omega) = \langle r_{\text{out},2}\rangle_\omega / \langle r_{\text{in},1}\rangle_\omega = \sqrt{\kappa_2}\langle a\rangle_\omega / \alpha_0 u(\omega)$ are the reflection and transmission coefficients with $\langle \mathcal{O}\rangle_\omega = \int dt\, e^{i\omega t}\langle \mathcal{O}\rangle_t$.

To derive the transmission $T(\omega)$ conditioned on the qubit state $|s\rangle$, we now find $\langle a\rangle_\omega$ from the quantum Langevin equation for $\langle a\rangle_t$,

$$\langle \dot{a}\rangle_t = -\frac{\kappa}{2}\langle a\rangle_t + \tilde{g}_1(t)s - \sqrt{\kappa_1}\alpha_0 u(t). \tag{2}$$

The displacement of the cavity vacuum due to the interaction $\propto \tilde{g}_1(t)$ can therefore be canceled exactly, conditioned on the qubit being in state $|1\rangle$, by ensuring that $\sqrt{\kappa_1}\alpha_0 u(t) = \tilde{g}_1(t)$. Destructive interference then precludes a transfer of photons to the output transmission line, leading to perfect reflection of the input field. Evidence of such destructive interference was recently observed experimentally in Ref. [66], where a modulated longitudinal coupling and a cavity drive were both generated with a common voltage source (acting as a common phase reference). Because the input state is a coherent state [and coherent states are eigenstates of $r_{\text{in},1}(t)$], there are no quantum fluctuations about the average dynamics $\langle r_{\text{in},1}\rangle_t = \alpha_0 u(t)$. For a nonideal input, however, fluctuations about the average ($\alpha_0 \to \alpha_0 + \delta\alpha$) lead to imperfect cancellation for $s = 1$.

For a cavity that is initially empty, we have $\langle a\rangle_0 = 0$. Integrating the quantum Langevin equation [Eq. (2)] with this initial condition gives

$$\langle a\rangle_\omega = \chi_c(\omega)[\tilde{g}_1(\omega)s - \sqrt{\kappa_1}\alpha_0 u(\omega)], \tag{3}$$

where $\chi_c(\omega) = (\kappa/2 - i\omega)^{-1}$. For $\sqrt{\kappa_1}\alpha_0 u(\omega) = \tilde{g}_1(\omega)$, the transmission can then be written as

$$T(\omega) = (1 - s)\frac{\sqrt{\kappa_1\kappa_2}}{i\omega - \kappa/2}. \tag{4}$$

The input pulse $u(\omega)$ has support for $\omega \lesssim 1/\tau$ localized about the cavity frequency (corresponding to $\omega = 0$ in the rotating frame). Near-perfect transmission can then be achieved for $s = 0$ and $\kappa_1 = \kappa_2 = \kappa/2$ by operating in the regime of large $\kappa\tau$, where $\chi_c(\omega)$ is much broader in frequency than $u(\omega)$. Finite-bandwidth effects for a Gaussian input waveform $u(t)$ may be neglected provided [51]

$N = |\alpha_0|^2 \ll (\kappa\tau)^4$. Given $T(\omega)$ for a fixed value of s, $R(\omega)$ is related to $T(\omega)$ through the input-output relation, $\sqrt{\kappa_2}[R(\omega) - 1] = \sqrt{\kappa_1}T(\omega)$.

An alternative way to condition the cavity transmission on the state of a qubit would be to engineer a qubit-state-dependent shift of the cavity frequency using dispersive coupling $\chi\sigma_z a^\dagger a$, where $2|\chi| \gg \kappa$. A narrow-band input tone at frequency χ would then be transmitted conditioned on state $|0\rangle$ and reflected for state $|1\rangle$. However, in the dispersive regime ($\epsilon = |g_\perp/\delta| < 1$), this necessarily requires (very) strong coupling $|g_\perp| \gg \kappa/\epsilon$. The entangler presented here, by contrast, can be operated even if $|\tilde{g}_1| \lesssim \kappa$. Dipole-induced transparency [67] and reflection [68] also result in perfect steady-state transmission or reflection of a weak input pulse conditional on the presence of a resonant, transversally coupled dipole. These effects are not, however, QND in the state of the decoupled dipole and furthermore require that the cavity be driven with an average of $N_{\rm cav} \lesssim 1$ intracavity photon [69]. For the entangler presented here, by contrast, the transmission vs reflection of a transient pulse is QND; it is conditioned on the decoupled qubit state $|s\rangle$. Moreover, the entangler works in the regime $N_{\rm cav} \sim N/(\kappa\tau) > 1$, provided the finite-bandwidth condition is satisfied [$N \ll (\kappa\tau)^4$ for a Gaussian waveform].

The qubit-state-conditioned transmission [Eq. (4)] can be used to generate entangled states. To describe the states associated with the reflected and transmitted fields, we use the virtual-cavity formalism of Refs. [63,64] to recast the input, reflected, and transmitted wave packets as the fields emitted from—or absorbed into—fictitious (virtual) single-sided cavities coupled to the transmission lines via time-dependent couplings. This formalism allows for an efficient description of the scattering of an input pulse into prespecified spatiotemporal modes, which can be modeled as the modes of virtual cavities. Accounting for the input pulse, cavity field, reflected pulse, and transmitted pulse, the evolution of the cavity and transmission lines is then fully described by an effective four-mode model. The quantum master equation governing this evolution is [63,64]

$$\dot{\rho}_\xi = -i[H_0(t) + V(t), \rho_\xi] + \sum_{i=1,2} \mathcal{D}[L_i]\rho_\xi, \tag{5}$$

where ρ_ξ is the density matrix conditioned on a realization of the noise $\xi(t)$, and where

$$V(t) = \frac{i}{2}\Big[\sqrt{\kappa_1}\lambda_u^*(t)a_u^\dagger a + \sum_{i=1,2}\sqrt{\kappa_i}\,\lambda_{v_i}(t)a^\dagger a_{v_i} + \lambda_u^*(t)\lambda_{v_1}(t)a_u^\dagger a_{v_1} - \text{H.c.}\Big]. \tag{6}$$

In Eq. (5), $\mathcal{D}[L]\rho = L\rho L^\dagger - \frac{1}{2}\{L^\dagger L, \rho\}$ is a damping superoperator. The operators $L_1 = \sum_{\mu=u,v_1}\lambda_\mu(t)a_\mu + \sqrt{\kappa_1}a$ and $L_2 = \lambda_{v_2}(t)a_{v_2} + \sqrt{\kappa_2}a$ model decay from the virtual cavity modes a_μ, as well as decay out of the cavity mode a with rate $\kappa = \kappa_1 + \kappa_2$. The couplings to the virtual cavities are given by $\lambda_u(t) = u(t)/(\int_t^\infty dt'|u(t')|^2)^{1/2}$ and $\lambda_{v_i}(t) = (-1)^i v_i(t)/(\int_0^t dt'|v_i(t')|^2)^{1/2}$ [63,64,70]. The i-dependent sign in λ_{v_i} reflects the fact that in our model, a transmitted pulse undergoes a π phase shift [cf Eq. (4)]. The couplings $\lambda_u(t)$ and $\lambda_{v_i}(t)$ have singularities at $t \to \infty$ and $t = 0$, respectively, and, for real cavities, both $\lambda_u(t)$ and $\lambda_{v_i}(t)$ would have to be truncated to finite values to realize absorption (emission) into (out of) a chosen spatiotemporal mode [70]. In the virtual-cavity formalism, however, these unphysical couplings are abstractions used to calculate the dynamics into (or out of) of a chosen mode. No additional (real) cavities or time-dependent couplings are required to realize the entangler.

We assume a fast $\pi/2$ pulse can be used to prepare the qubit in the ($t = 0$) initial state $|+\rangle = (|1\rangle + |0\rangle)/\sqrt{2}$, with the cavity in the vacuum state ($\langle a\rangle_0 = 0$). A coherent-state wave packet then evolves from the input mode a_u to the two output modes a_{v_i} ($i = 1, 2$). For times $t \gg \tau$ exceeding the duration of the input pulse, the quantum states associated with the reflected and transmitted waveforms $v_i(t)$, conditioned on s, will have been fully transferred into their respective fictitious cavities: $\alpha_{is} = \lim_{t\to\infty}\langle a_{v_i}\rangle_t = (-1)^{i-1}\alpha_0\int(d\omega/2\pi)|v_i(\omega)|^2$. The joint state of the qubit and transmission lines, found from a direct integration of Eq. (5), is then $\rho(t) = \langle\!\langle\rho_\xi(t)\rangle\!\rangle$, where $\langle\!\langle\rangle\!\rangle$ denotes an average over realizations of $\xi(t)$, and where $\rho_\xi(t) = |\Psi_{\xi(t)}\rangle\langle\Psi_{\xi(t)}|$ with

$$|\Psi_{\xi(t)}\rangle = \frac{1}{\sqrt{2}}\left(e^{\frac{i}{2}\theta_\xi(t)}|1,\psi_1\rangle + e^{-\frac{i}{2}\theta_\xi(t)}|0,\psi_0\rangle\right). \tag{7}$$

Here, $\theta_\xi(t) = \int_0^t dt'\xi(t')$ is a random phase, $|\psi_s\rangle = \prod_{i=1,2} D_i(\alpha_{is})|\text{vac}\rangle$ is the state of the transmission lines conditioned on s, $|\text{vac}\rangle$ is the vacuum, and $D_i(\alpha) = \exp\{\alpha a_{v_i}^\dagger - \text{H.c.}\}$ is a displacement operator. For $\kappa_1 = \kappa_2 = \kappa/2$ and up to corrections in $N/(\kappa\tau)^4 \ll 1$, only one of α_{is} is nonzero for each value of s: For $s = 1$, $\alpha_{11} = \alpha_0$ and $\alpha_{21} = 0$, while for $s = 0$, $\alpha_{10} = 0$ and $\alpha_{20} = -\alpha_0$. Equation (7) therefore describes a photonic which-path qubit entangled with the control qubit (a QWP state). Under the same finite-bandwidth conditions, imperfections in the input source such that $\alpha_0 \to \alpha_0 + \delta\alpha$ will lead instead to $\alpha_{11} = \alpha_0$, $\alpha_{21} = -\delta\alpha$, $\alpha_{10} = 0$, and $\alpha_{20} = -(\alpha_0 + \delta\alpha)$. This follows from integrating the Langevin equation [Eq. (2)] with $\alpha_0 \to \alpha_0 + \delta\alpha$ and solving for the reflected and transmitted fields. If we take $\delta\alpha$ to be a complex-valued, zero-mean Gaussian random variable, then the fidelity of the ideal QWP state [Eq. (7) with $\xi = 0$] with respect to the mixed state obtained by averaging over $\delta\alpha$ is $e^{-\langle|\delta\alpha|^2\rangle_{\delta\alpha}}$, where here, $\langle\rangle_{\delta\alpha}$ describes an average over $\delta\alpha$. High-fidelity QWP states therefore require a stable

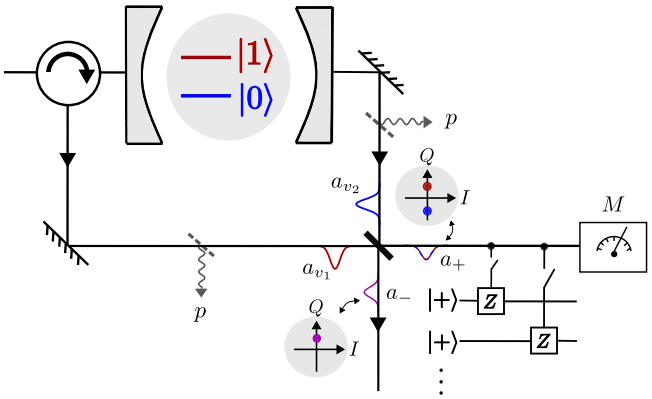

FIG. 2. An interferometry setup can be used to entangle the which-path degree of freedom with a target qubit initialized in $|+\rangle$ via a conditional phase shift: $Z|+\rangle = |-\rangle$. This can be accomplished by reencoding the which-path degree of freedom in the photon-number parity of a cat state (composed of a superposition of two distinct coherent states occupying the spatiotemporal mode annihilated by a_+) propagating to the right of the 50:50 beam splitter. The symbol labeled M represents a measurement of the quadrature Q, which can be used to prepare an m-qubit GHZ state (or Bell state for $m = 2$) involving the control qubit and $(m-1)$ target qubits. Photon loss occurring with probability p is modeled with fictitious beam splitters having reflectivity p.

coherent-state source with a low absolute noise level, below one photon per pulse ($\langle|\delta\alpha|^2\rangle_{\delta\alpha} \ll 1$).

Entanglement distribution.—The which-path degree of freedom can be entangled with a second ("target") qubit for long-range entanglement distribution. Crucially, this also provides a direct avenue for quantifying entanglement in QWP states through measurements of stationary qubits only. The setup is illustrated schematically in Fig. 2. By interfering the reflected and transmitted fields at a 50:50 beam splitter, the output modes can be mapped to new modes $a_\pm$ such that $\langle a_{\pm,s}\rangle = (\alpha_{1s} \pm \alpha_{2s})/\sqrt{2}$. This gives $\langle a_{-,s}\rangle = \alpha$ independent of s, where $\alpha = \alpha_0/\sqrt{2}$. The a_+ mode, by contrast, has s dependence given by $\langle a_{+,s}\rangle = (2s-1)\alpha$. The beam splitter consequently reencodes the which-path degree of freedom in the phase of the coherent-state amplitude: $\langle a_{+,1}\rangle = +\alpha$ and $\langle a_{+,0}\rangle = -\alpha$.

For clarity, we now set $\xi(t) = 0$ for the purpose of explaining the protocol. The effects of dephasing [$\xi(t) \neq 0$] are included in the relevant result, Eq. (8), below. Since the a_- mode does not share entanglement with either the qubit or a_+ mode, it can be measured (traced over) without disturbing the state of the qubit and a_+ mode. The postmeasurement state is then $(1/2)\sum_{\lambda=\pm}\sqrt{\mathcal{N}_\lambda}|\lambda, C_\lambda\rangle$, where $|C_\pm\rangle = (|+\alpha\rangle \pm |-\alpha\rangle)/\sqrt{\mathcal{N}_\pm}$ are cat states (consisting of only even or odd photon-number states) and $\mathcal{N}_\pm$ are normalization factors. With the target qubit initialized in $|+\rangle$, the control and target qubits can be entangled through a phase flip on the target, $|+\rangle \to |-\rangle$, conditioned on an odd photon-number parity [51,71–74]. Following such a phase flip, the state of the qubits and electric field is $(1/2)\sum_{\lambda=\pm}\sqrt{\mathcal{N}_\lambda}|\lambda, \lambda, C_\lambda\rangle$. In the limit $\langle\alpha|-\alpha\rangle \to 0$, a final quadrature measurement of the electric field can then be used to project the qubits into the Bell state $(|++\rangle \pm |--\rangle)/\sqrt{2}$, conditioned on outcome $|\pm\alpha\rangle$. Multiqubit Greenberger-Horne-Zeilinger (GHZ) states $|+,+,\cdots,+\rangle \pm |-,-,\cdots,-\rangle$ can also be generated by allowing the field to interact sequentially with a series of potentially distant qubits. In contrast to the well-established single-photon pitch-and-catch approach to long-range entanglement distribution, involving the emission and destructive reabsorption of a single photon [13–19], the approach presented here is QND in the photon number and therefore provides a clear path towards the generation of multipartite entangled states.

We can quantify the effects of photon loss on the amount of distributed entanglement by inserting a fictitious beam splitter, described by the unitary $B_{c,c'}(\varphi) = e^{i\varphi(c^\dagger c' + \text{H.c.})}$ [28], into each arm of the interferometer (Fig. 2). With $c = a_{v_i}$, this describes scattering from a_{v_i} into loss mode a'_{v_i} (in the environment) with probability $p = \cos^2\varphi$. Tracing over the loss modes $a'_{v_{1,2}}$ then yields a reduced density matrix for the state of the qubit and modes $a_{v_{1,2}}$. In the presence of such loss, and for finite coherent-state overlap $\langle\alpha|-\alpha\rangle \neq 0$, the postmeasurement state of the qubits is not an ideal Bell state, but is instead mixed: For a measurement of the electric field along the quadrature Q of coherent-state displacement [75], the postmeasurement state of the qubits (conditioned on an inferred displacement along $\pm Q$) is an X state [76] whose concurrence C [77–79] can easily be computed [51]:

$$C(t) = \max\{0, \operatorname{erf}(\sqrt{N_\eta})e^{-N_p - \chi_\xi(t)} - \operatorname{erfc}(\sqrt{N_\eta})\}, \tag{8}$$

where $N_p = pN = p|\alpha_0|^2$ and $N_\eta = \eta(1-p)N$ are controlled by the average number of photons lost and detected, respectively. Here, $\eta \in (0, 1]$ is the detector efficiency, and

$$\chi_\xi(t) = \int \frac{d\omega}{2\pi} \frac{4\sin^2(\frac{\omega t}{2})}{\omega^2} S(\omega) \tag{9}$$

results from an average $\langle\langle\rangle\rangle$ over realizations of the noise $\xi(t)$, here taken to be stationary, zero-mean Gaussian noise with spectral density $S(\omega) = \int dt\, e^{-i\omega t}\langle\langle\xi(t)\xi(0)\rangle\rangle$. The concurrence [Eq. (8)] quantifies the amount of entanglement that can be distributed to a second qubit in the presence of (symmetric) photon loss in the interferometer, qubit dephasing, and imperfect assignment fidelity at the final measurement of the electric field. In particular, the expression for $C(t)$ indicates that for fixed values of p and η, there is an optimal N that maximizes the entanglement [51]. In the presence of asymmetric losses with probabilities p_1 and p_2, Eq. (8) with $p = \max\{p_1, p_2\}$ provides a lower bound on the achievable concurrence.

The requirement $\sqrt{\kappa/2}\alpha_0 u(t) = \tilde{g}_1(t)$ limits the average number of photons in the input coherent state. For a Gaussian $u(t)$, $N = |\alpha_0|^2 = 2\sqrt{\pi}(\tilde{g}_1^{\max})^2\tau/\kappa$, where $\tilde{g}_1^{\max} = \max_t |\tilde{g}_1(t)|$. Together with the bandwidth requirement $N \ll (\kappa\tau)^4$, this implies that $N \ll N_{\max} \equiv (\tilde{g}_1^{\max}\tau)^{8/5}$. A larger τ therefore increases $N_{\max}$. However, the pulse duration is also subject to the requirement $\tau < T_2^*$, where T_2^* is the dephasing time of the qubit [defined by $\chi_\xi(T_2^*) = 1$]. For example, if $g_1^{\max}/2\pi = 1$ MHz and $\tau = 1$ μs, then $N_{\max} \simeq 19$. For $\tilde{g}_1/\kappa = 1/8$ (weak coupling), we then have $N \simeq 3$, close to the value that maximizes the two-qubit concurrence ($C \simeq 0.95$) for $p = 0.01$ [51]. This scenario may be realistic for, e.g., an electron-spin qubit in a silicon DQD with a magnetic field gradient. The longitudinal coupling for this case can be comparable to the transverse coupling ∼1–10 MHz [42]. Dephasing times for electron-spin qubits in ^{28}Si quantum dots reach $T_2^* \sim 100\ \mu\text{s} \gg \tau$ [80]. The same values of N and $N_{\max}$ could also be realized for flux-tunable transmons, with a longitudinal coupling ∼10 MHz [41] and pulse duration $\tau \sim 100$ ns $\ll T_2^*$ (for transmons, coherence times reach $T_2^* \simeq 100$ μs [81]).

Precision metrology.—The entangler described above can also be used to perform quantum-enhanced precision measurements of a phase ϕ acquired by the field reflected from the cavity as it propagates along arm 1 of an interferometer (Fig. 2). The fundamental precision bound for estimation of ϕ (the quantum Cramér-Rao bound [82,83]) is better for QWP states than for either NOON states (superpositions of N-photon Fock states, one in each interferometer arm) or entangled coherent states [27] (similarly, superpositions of coherent states) having the same average number N of photons [84].

Outlook.—The entangler presented here could also be used to perform measurements of the phase acquired by the control qubit. Specifically, a modulated longitudinal coupling, followed by a rapid reset [85–88] $|0\rangle \to |1\rangle$, can be used to map the relative phase $|0\rangle + e^{i\theta}|1\rangle$ of the initial qubit state onto the state $|-\alpha\rangle + e^{i\theta}|\alpha\rangle$ of the a_+ mode. A projective measurement of $|C_\pm\rangle$ then yields a single bit of information about θ (the maximum achievable for a single-shot qubit readout). This may be useful in situations where θ encodes information about dynamics induced by a classical or quantum environment [89,90].

We thank A. Blais and K. Wang for useful discussions. We also acknowledge funding from the Natural Sciences and Engineering Research Council (NSERC) and from the Fonds de recherche du Québec—Nature et technologies (FRQNT).

*zoe.mcintyre@mail.mcgill.ca
†william.coish@mcgill.ca

[1] T. E. Northup and R. Blatt, Quantum information transfer using photons, Nat. Photonics **8**, 356 (2014).
[2] A. Reiserer and G. Rempe, Cavity-based quantum networks with single atoms and optical photons, Rev. Mod. Phys. **87**, 1379 (2015).
[3] L. M. K. Vandersypen, H. Bluhm, J. S. Clarke, A. S. Dzurak, R. Ishihara, A. Morello, D. J. Reilly, L. R. Schreiber, and M. Veldhorst, Interfacing spin qubits in quantum dots and donors–hot, dense, and coherent, npj Quantum Inf. **3**, 34 (2017).
[4] D. Awschalom, K. K. Berggren, H. Bernien, S. Bhave, L. D. Carr, P. Davids, S. E. Economou, D. Englund, A. Faraon, M. Fejer *et al.*, Development of quantum interconnects (QuICs) for next-generation information technologies, PRX Quantum **2**, 017002 (2021).
[5] M. Ruf, N. H. Wan, H. Choi, D. Englund, and R. Hanson, Quantum networks based on color centers in diamond, J. Appl. Phys. **130**, 070901 (2021).
[6] L.-M. Duan, B. B. Blinov, D. L. Moehring, and C. Monroe, Scalable trapped ion quantum computation with a probabilistic ion-photon mapping, Quantum Inf. Comput. **4**, 165 (2004).
[7] J. Hofmann, M. Krug, N. Ortegel, L. Gérard, M. Weber, W. Rosenfeld, and H. Weinfurter, Heralded entanglement between widely separated atoms, Science **337**, 72 (2012).
[8] H. Bernien, B. Hensen, W. Pfaff, G. Koolstra, M. S. Blok, L. Robledo, T. H. Taminiau, M. Markham, D. J. Twitchen, L. Childress, and R. Hanson, Heralded entanglement between solid-state qubits separated by three metres, Nature (London) **497**, 86 (2013).
[9] B. Hensen, H. Bernien, A. E. Dréau, A. Reiserer, N. Kalb, M. S. Blok, J. Ruitenberg, R. F. L. Vermeulen, R. N. Schouten, C. Abellán *et al.*, Loophole-free Bell inequality violation using electron spins separated by 1.3 kilometres, Nature (London) **526**, 682 (2015).
[10] A. Delteil, Z. Sun, W.-b. Gao, E. Togan, S. Faelt, and A. Imamoğlu, Generation of heralded entanglement between distant hole spins, Nat. Phys. **12**, 218 (2016).
[11] A. Narla, S. Shankar, M. Hatridge, Z. Leghtas, K. M. Sliwa, E. Zalys-Geller, S. O. Mundhada, W. Pfaff, L. Frunzio, R. J. Schoelkopf *et al.*, Robust concurrent remote entanglement between two superconducting qubits, Phys. Rev. X **6**, 031036 (2016).
[12] M. Pompili, S. L. N. Hermans, S. Baier, H. K. C. Beukers, P. C. Humphreys, R. N. Schouten, R. F. L. Vermeulen, M. J. Tiggelman, L. dos Santos Martins, B. Dirkse, S. Wehner, and R. Hanson, Realization of a multinode quantum network of remote solid-state qubits, Science **372**, 259 (2021).
[13] J. I. Cirac, P. Zoller, H. J. Kimble, and H. Mabuchi, Quantum state transfer and entanglement distribution among distant nodes in a quantum network, Phys. Rev. Lett. **78**, 3221 (1997).
[14] S. Ritter, C. Nölleke, C. Hahn, A. Reiserer, A. Neuzner, M. Uphoff, M. Mücke, E. Figueroa, J. Bochmann, and G. Rempe, An elementary quantum network of single atoms in optical cavities, Nature (London) **484**, 195 (2012).
[15] P. Kurpiers, P. Magnard, T. Walter, B. Royer, M. Pechal, J. Heinsoo, Y. Salathé, A. Akin, S. Storz, J.-C. Besse *et al.*, Deterministic quantum state transfer and remote entanglement using microwave photons, Nature (London) **558**, 264 (2018).

[16] C. J. Axline, L. D. Burkhart, W. Pfaff, M. Zhang, K. Chou, P. Campagne-Ibarcq, P. Reinhold, L. Frunzio, S. M. Girvin, L. Jiang *et al.*, On-demand quantum state transfer and entanglement between remote microwave cavity memories, Nat. Phys. **14**, 705 (2018).
[17] P. Campagne-Ibarcq, E. Zalys-Geller, A. Narla, S. Shankar, P. Reinhold, L. Burkhart, C. Axline, W. Pfaff, L. Frunzio, R. J. Schoelkopf *et al.*, Deterministic remote entanglement of superconducting circuits through microwave two-photon transitions, Phys. Rev. Lett. **120**, 200501 (2018).
[18] N. Leung, Y. Lu, S. Chakram, R. K. Naik, N. Earnest, R. Ma, K. Jacobs, A. N. Cleland, and D. I. Schuster, Deterministic bidirectional communication and remote entanglement generation between superconducting qubits, npj Quantum Inf. **5**, 18 (2019).
[19] P. Magnard, S. Storz, P. Kurpiers, J. Schär, F. Marxer, J. Lütolf, T. Walter, J.-C. Besse, M. Gabureac, K. Reuer *et al.*, Microwave quantum link between superconducting circuits housed in spatially separated cryogenic systems, Phys. Rev. Lett. **125**, 260502 (2020).
[20] Y. Zhong, H.-S. Chang, A. Bienfait, É. Dumur, M.-H. Chou, C. R. Conner, J. Grebel, R. G. Povey, H. Yan, D. I. Schuster *et al.*, Deterministic multi-qubit entanglement in a quantum network, Nature (London) **590**, 571 (2021).
[21] U. L. Andersen, J. S. Neergaard-Nielsen, P. Van Loock, and A. Furusawa, Hybrid discrete-and continuous-variable quantum information, Nat. Phys. **11**, 713 (2015).
[22] S. Takeda, M. Fuwa, P. van Loock, and A. Furusawa, Entanglement swapping between discrete and continuous variables, Phys. Rev. Lett. **114**, 100501 (2015).
[23] K. Huang, H. Le Jeannic, O. Morin, T. Darras, G. Guccione, A. Cavaillès, and J. Laurat, Engineering optical hybrid entanglement between discrete-and continuous-variable states, New J. Phys. **21**, 083033 (2019).
[24] G. Guccione, T. Darras, H. Le Jeannic, V. B. Verma, S. W. Nam, A. Cavaillès, and J. Laurat, Connecting heterogeneous quantum networks by hybrid entanglement swapping, Sci. Adv. **6**, eaba4508 (2020).
[25] I. B. Djordjevic, Hybrid CV-DV quantum communications and quantum networks, IEEE Access **10**, 23284 (2022).
[26] T. Darras, B. E. Asenbeck, G. Guccione, A. Cavaillès, H. Le Jeannic, and J. Laurat, A quantum-bit encoding converter, Nat. Photonics **17**, 165 (2023).
[27] B. C. Sanders, Entangled coherent states, Phys. Rev. A **45**, 6811 (1992).
[28] J. Joo, W. J. Munro, and T. P. Spiller, Quantum metrology with entangled coherent states, Phys. Rev. Lett. **107**, 083601 (2011).
[29] J. J. Bollinger, W. M. Itano, D. J. Wineland, and D. J. Heinzen, Optimal frequency measurements with maximally correlated states, Phys. Rev. A **54**, R4649 (1996).
[30] H. Lee, P. Kok, and J. P. Dowling, A quantum Rosetta stone for interferometry, J. Mod. Opt. **49**, 2325 (2002).
[31] V. Giovannetti, S. Lloyd, and L. Maccone, Advances in quantum metrology, Nat. Photonics **5**, 222 (2011).
[32] M. A. Taylor and W. P. Bowen, Quantum metrology and its application in biology, Phys. Rep. **615**, 1 (2016).
[33] P.-A. Moreau, E. Toninelli, T. Gregory, and M. J. Padgett, Imaging with quantum states of light, Nat. Rev. Phys. **1**, 367 (2019).
[34] S. Mukamel, M. Freyberger, W. Schleich, M. Bellini, A. Zavatta, G. Leuchs, C. Silberhorn, R. W. Boyd, L. L. Sánchez-Soto, A. Stefanov *et al.*, Roadmap on quantum light spectroscopy, J. Phys. B **53**, 072002 (2020).
[35] R. Schnabel, N. Mavalvala, D. E. McClelland, and P. K. Lam, Quantum metrology for gravitational wave astronomy, Nat. Commun. **1**, 121 (2010).
[36] J. Aasi, J. Abadie, B. P. Abbott, R. Abbott, T. D. Abbott, M. R. Abernathy, C. Adams, T. Adams, P. Addesso, R. X. Adhikari *et al.*, Enhanced sensitivity of the LIGO gravitational wave detector by using squeezed states of light, Nat. Photonics **7**, 613 (2013).
[37] M. Tse, H. Yu, N. Kijbunchoo, A. Fernandez-Galiana, P. Dupej, L. Barsotti, C. D. Blair, D. D. Brown, S. E. Dwyer, A. Effler *et al.*, Quantum-enhanced advanced LIGO detectors in the era of gravitational-wave astronomy, Phys. Rev. Lett. **123**, 231107 (2019).
[38] H. Yu, L. McCuller, M. Tse, N. Kijbunchoo, L. Barsotti, and N. Mavalvala, Quantum correlations between light and the kilogram-mass mirrors of LIGO, Nature (London) **583**, 43 (2020).
[39] A. J. Kerman, Quantum information processing using quasiclassical electromagnetic interactions between qubits and electrical resonators, New J. Phys. **15**, 123011 (2013).
[40] P.-M. Billangeon, J. S. Tsai, and Y. Nakamura, Circuit-QED-based scalable architectures for quantum information processing with superconducting qubits, Phys. Rev. B **91**, 094517 (2015).
[41] N. Didier, J. Bourassa, and A. Blais, Fast quantum nondemolition readout by parametric modulation of longitudinal qubit-oscillator interaction, Phys. Rev. Lett. **115**, 203601 (2015).
[42] F. Beaudoin, D. Lachance-Quirion, W. A. Coish, and M. Pioro-Ladrière, Coupling a single electron spin to a microwave resonator: Controlling transverse and longitudinal couplings, Nanotechnology **27**, 464003 (2016).
[43] S. Richer and D. DiVincenzo, Circuit design implementing longitudinal coupling: A scalable scheme for superconducting qubits, Phys. Rev. B **93**, 134501 (2016).
[44] S. Richer, N. Maleeva, S. T. Skacel, I. M. Pop, and D. DiVincenzo, Inductively shunted transmon qubit with tunable transverse and longitudinal coupling, Phys. Rev. B **96**, 174520 (2017).
[45] S. P. Harvey, C. G. L. Bøttcher, L. A. Orona, S. D. Bartlett, A. C. Doherty, and A. Yacoby, Coupling two spin qubits with a high-impedance resonator, Phys. Rev. B **97**, 235409 (2018).
[46] N. Lambert, M. Cirio, M. Delbecq, G. Allison, M. Marx, S. Tarucha, and F. Nori, Amplified and tunable transverse and longitudinal spin-photon coupling in hybrid circuit-QED, Phys. Rev. B **97**, 125429 (2018).
[47] S. Bosco, P. Scarlino, J. Klinovaja, and D. Loss, Fully tunable longitudinal spin-photon interactions in Si and Ge quantum dots, Phys. Rev. Lett. **129**, 066801 (2022).
[48] C. G. L. Bøttcher, S. P. Harvey, S. Fallahi, G. C. Gardner, M. J. Manfra, U. Vool, S. D. Bartlett, and A. Yacoby, Parametric longitudinal coupling between a high-impedance superconducting resonator and a semiconductor quantum dot singlet-triplet spin qubit, Nat. Commun. **13**, 4773 (2022).

[49] V. P. Michal, J. C. Abadillo-Uriel, S. Zihlmann, R. Maurand, Y.-M. Niquet, and M. Filippone, Tunable hole spin-photon interaction based on g-matrix modulation, Phys. Rev. B **107**, L041303 (2023).
[50] Y. Fang, P. Philippopoulos, D. Culcer, W. A. Coish, and S. Chesi, Recent advances in hole-spin qubits, Mater. Quantum Technol. **3**, 012003 (2023).
[51] See Supplemental Material at http://link.aps.org/supplemental/10.1103/PhysRevLett.132.093603, which includes Refs. [52–62], for a derivation of longitudinal coupling for spin and charge qubits, a discussion of finite-bandwidth corrections to the QWP state fidelity, and a derivation of the two-qubit concurrence.
[52] X. Mi, J. V. Cady, D. M. Zajac, P. W. Deelman, and J. R. Petta, Strong coupling of a single electron in silicon to a microwave photon, Science **355**, 156 (2017).
[53] A. J. Landig, J. V. Koski, P. Scarlino, U. Mendes, A. Blais, C. Reichl, W. Wegscheider, A. Wallraff, K. Ensslin, and T. Ihn, Coherent spin–photon coupling using a resonant exchange qubit, Nature (London) **560**, 179 (2018).
[54] N. Samkharadze, G. Zheng, N. Kalhor, D. Brousse, A. Sammak, U. Mendes, A. Blais, G. Scappucci, and L. Vandersypen, Strong spin-photon coupling in silicon, Science **359**, 1123 (2018).
[55] I. Seidler, T. Struck, R. Xue, N. Focke, S. Trellenkamp, H. Bluhm, and L. R. Schreiber, Conveyor-mode single-electron shuttling in Si/SiGe for a scalable quantum computing architecture, npj Quantum Inf. **8**, 100 (2022).
[56] L. Childress, A. S. Sørensen, and M. D. Lukin, Mesoscopic cavity quantum electrodynamics with quantum dots, Phys. Rev. A **69**, 042302 (2004).
[57] K. D. Petersson, J. R. Petta, H. Lu, and A. C. Gossard, Quantum coherence in a one-electron semiconductor charge qubit, Phys. Rev. Lett. **105**, 246804 (2010).
[58] R. Schoelkopf and S. Girvin, Wiring up quantum systems, Nature (London) **451**, 664 (2008).
[59] A. Imamoğlu, Cavity QED based on collective magnetic dipole coupling: Spin ensembles as hybrid two-level systems, Phys. Rev. Lett. **102**, 083602 (2009).
[60] G. Burkard, T. D. Ladd, A. Pan, J. M. Nichol, and J. R. Petta, Semiconductor spin qubits, Rev. Mod. Phys. **95**, 025003 (2023).
[61] Y. M. Zhang, X. W. Li, W. Yang, and G. R. Jin, Quantum Fisher information of entangled coherent states in the presence of photon loss, Phys. Rev. A **88**, 043832 (2013).
[62] T. Yu and J. H. Eberly, Quantum open system theory: Bipartite aspects, Phys. Rev. Lett. **97**, 140403 (2006).
[63] A. H. Kiilerich and K. Mølmer, Input-output theory with quantum pulses, Phys. Rev. Lett. **123**, 123604 (2019).
[64] A. H. Kiilerich and K. Mølmer, Quantum interactions with pulses of radiation, Phys. Rev. A **102**, 023717 (2020).
[65] C. W. Gardiner and M. J. Collett, Input and output in damped quantum systems: Quantum stochastic differential equations and the master equation, Phys. Rev. A **31**, 3761 (1985).
[66] J. Corrigan, B. Harpt, N. Holman, R. Ruskov, P. Marciniec, D. Rosenberg, D. Yost, R. Das, W. D. Oliver, R. McDermott *et al.*, Longitudinal coupling between a Si/SiGe quantum dot and an off-chip TiN resonator, Phys. Rev. Appl. **20**, 064005 (2023).
[67] E. Waks and J. Vuckovic, Dipole-induced transparency in drop-filter cavity-waveguide systems, Phys. Rev. Lett. **96**, 153601 (2006).
[68] A. Auffèves-Garnier, C. Simon, J.-M. Gérard, and J.-P. Poizat, Giant optical nonlinearity induced by a single two-level system interacting with a cavity in the Purcell regime, Phys. Rev. A **75**, 053823 (2007).
[69] D. Englund, A. Faraon, I. Fushman, N. Stoltz, P. Petroff, and J. Vuckovic, Controlling cavity reflectivity with a single quantum dot, Nature (London) **450**, 857 (2007).
[70] H. I. Nurdin, M. R. James, and N. Yamamoto, Perfect single device absorber of arbitrary traveling single photon fields with a tunable coupling parameter: A QSDE approach, in *Proceedings of the 2016 IEEE 55th Conference on Decision and Control (CDC)* (IEEE, New York, 2016), pp. 2513–2518.
[71] J.-C. Besse, S. Gasparinetti, M. C. Collodo, T. Walter, P. Kurpiers, M. Pechal, C. Eichler, and A. Wallraff, Single-shot quantum nondemolition detection of individual itinerant microwave photons, Phys. Rev. X **8**, 021003 (2018).
[72] S. Kono, K. Koshino, Y. Tabuchi, A. Noguchi, and Y. Nakamura, Quantum non-demolition detection of an itinerant microwave photon, Nat. Phys. **14**, 546 (2018).
[73] B. Hacker, S. Welte, S. Daiss, A. Shaukat, S. Ritter, L. Li, and G. Rempe, Deterministic creation of entangled atom–light Schrödinger-cat states, Nat. Photonics **13**, 110 (2019).
[74] J.-C. Besse, S. Gasparinetti, M. C. Collodo, T. Walter, A. Remm, J. Krause, C. Eichler, and A. Wallraff, Parity detection of propagating microwave fields, Phys. Rev. X **10**, 011046 (2020).
[75] A. Dragan and K. Banaszek, Homodyne Bell's inequalities for entangled mesoscopic superpositions, Phys. Rev. A **63**, 062102 (2001).
[76] T. Yu and J. H. Eberly, Evolution from entanglement to decoherence of bipartite mixed "X" states, Quantum Inf. Comput. **7**, 459 (2007).
[77] S. A. Hill and W. K. Wootters, Entanglement of a pair of quantum bits, Phys. Rev. Lett. **78**, 5022 (1997).
[78] W. K. Wootters, Entanglement of formation of an arbitrary state of two qubits, Phys. Rev. Lett. **80**, 2245 (1998).
[79] W. K. Wootters, Entanglement of formation and concurrence, Quantum Inf. Comput. **1**, 27 (2001).
[80] P. Stano and D. Loss, Review of performance metrics of spin qubits in gated semiconducting nanostructures, Nat. Rev. Phys. **4**, 672 (2022).
[81] M. Kjaergaard, M. E. Schwartz, J. Braumüller, P. Krantz, J. I.-J. Wang, S. Gustavsson, and W. D. Oliver, Superconducting qubits: Current state of play, Annu. Rev. Condens. Matter Phys. **11**, 369 (2020).
[82] S. L. Braunstein and C. M. Caves, Statistical distance and the geometry of quantum states, Phys. Rev. Lett. **72**, 3439 (1994).
[83] S. L. Braunstein, C. M. Caves, and G. J. Milburn, Generalized uncertainty relations: Theory, examples, and Lorentz invariance, Ann. Phys. (N.Y.) **247**, 135 (1996).
[84] Z. M. McIntyre and W. A. Coish (to be published).
[85] M. D. Reed, B. R. Johnson, A. A. Houck, L. DiCarlo, J. M. Chow, D. I. Schuster, L. Frunzio, and R. J. Schoelkopf,

Fast reset and suppressing spontaneous emission of a superconducting qubit, Appl. Phys. Lett. **96**, 203110 (2010).

[86] J. E. Johnson, C. Macklin, D. H. Slichter, R. Vijay, E. B. Weingarten, J. Clarke, and I. Siddiqi, Heralded state preparation in a superconducting qubit, Phys. Rev. Lett. **109**, 050506 (2012).

[87] K. Geerlings, Z. Leghtas, I. M. Pop, S. Shankar, L. Frunzio, R. J. Schoelkopf, M. Mirrahimi, and M. H. Devoret, Demonstrating a driven reset protocol for a superconducting qubit, Phys. Rev. Lett. **110**, 120501 (2013).

[88] T. Kobayashi, T. Nakajima, K. Takeda, A. Noiri, J. Yoneda, and S. Tarucha, Feedback-based active reset of a spin qubit in silicon, npj Quantum Inf. **9**, 52 (2023).

[89] Z. McIntyre and W. A. Coish, Non-Markovian transient spectroscopy in cavity QED, Phys. Rev. Res. **4**, L042039 (2022).

[90] P. M. Mutter and G. Burkard, Fingerprints of qubit noise in transient cavity transmission, Phys. Rev. Lett. **128**, 236801 (2022).